applied sciences

MDPI

Article

Development of Simultaneous Dual-Resolution Digital Holography System

Xiaowan Zheng [1,2], Siyuan Fang [1], Bicheng Guo [1], Bernard Sia [3] and Lianxiang Yang [1,*]

1 Department of Mechanical Engineering, School of Engineering and Computer Science, Oakland University, Rochester, MI 48309, USA
2 College of Electrical and Information Engineering, Zhengzhou University of Light Industry, Zhengzhou 450002, China
3 US Army Ground Vehicle Systems Center, 6501 E 11 Mile Rd, Warren, MI 48397, USA
* Correspondence: yang2@oakland.edu

Abstract: This research paper is focused on the development of a digital holography system for simultaneous dual-resolution measurements. Digital holography has been widely used for deformation measurements and non-destructive testing (NDT) due to its advantages of high sensitivity, high accuracy, and whole-field, non-touch measurements. A traditional test only has one spatial resolution, which can cause a big deformation to be indistinguishable or minor defects to be ignored. Both large and small fields of view should be observed to reach a multi-spatial resolution measurement. Usually, multiple separate tests are used to observe the different sized fields of view, resulting in higher costs and longer required testing times. Furthermore, these tests may not be repeatable in some cases. This paper presents research on a novel digital holography system that achieves dual spatial resolution measurements simultaneously by testing different-sized fields of view with a single camera. The novel system has two optical channels with two optical layouts of holography to measure deformation. By changing the combined focus length, the two holographic setups have different fields of view, i.e., one has a large and the other has a small field of view. To realize a simultaneous test, the polarization technique is used to avoid cross-interference between the two optical layouts. Finally, spatial carrier fringes with different orientations are introduced into the two holographic setups by appropriately adjusting the reference beam of each setup. The different oriented spatial carrier fringes enable the spectrums of the two interferograms to be separated after a FT (Fourier transform) and the phase distributions of the two interferograms can be extracted and separated by windowing the spectrum to perform an IFT (inverse Fourier transform). The phase distributions can then be used to analyze and calculate the deformations. The experiment using this system is described in this paper and the practicability of this method is verified by the obtained experimental results.

Keywords: dual spatial resolution; speckle pattern interferometry; holographic interferometry; spatial phase shift method; polarization technology

Citation: Zheng, X.; Fang, S.; Guo, B.; Sia, B.; Yang, L. Development of Simultaneous Dual-Resolution Digital Holography System. *Appl. Sci.* **2023**, *13*, 2856. https://doi.org/10.3390/app13052856

Academic Editor: Martin Hagara

Received: 10 February 2023
Revised: 22 February 2023
Accepted: 22 February 2023
Published: 23 February 2023

1. Introduction

The digital holography interferometry technique is a non-contact, full-field, and highly sensitive optical measurement method. It is widely used in a variety of industrial areas, including the automotive and aerospace industries, for deformation/strain measurements and non-destructive testing (NDT) [1–6]. For this technique, one laser beam is split into two beams. One, called the object beam, illuminates the object's surface, while the other, called a reference beam, goes to a reference object, such as a mirror. These two beams meet at the CCD and interfere with each other on the CCD plane to produce an interferogram. The intensities of the interferograms can be recorded by a digital camera before and after loading. A visible fringe pattern, also called a hologram, that includes the object deformation information can be obtained to subtract the different intensity information and obtain deformation due to the applied load [7–10].

Currently, most optical inspection systems use a single camera with a fixed field of view to record images, resulting in only one resolution being obtained per measurement. However, some small defects may also be found without increasing the spatial resolution by improving the stability and the contrast of phase maps and avoiding air disturbances and environmental vibrations by a real-time phase processing method with high-frequency synchronizing trigger technology [11]. A high-spatial-resolution setup in combination with this technology would be even better for measuring smaller defects. Usually, one-resolution systems suffer from some disadvantages: (1) when measuring the deformation of an object with a strain concentration in some locations, the fringe pattern may be too dense to be resolved by the measurement system, which can cause the measurement to fail; (2) when conducting non-destructive testing, small-sized inner defects may be ignored due to a low spatial resolution. Measurements using different spatial resolutions would be necessary to solve these issues. Usually, separate multiple tests are used to observe different-sized fields of view. However, this will not only increase the labor costs and testing time, but also complicate the measurement operation. Furthermore, multiple measurements may not be achievable in some cases. Therefore, if a measurement is not repeatable, a simultaneous dual-resolution measurement system with different fields of view is helpful. To reach this goal, two optical channels with large and small fields of view are required to achieve a simultaneous dual spatial resolution measurement using one experimental setup.

Research on simultaneous measurement with two-channel systems has been reported, but almost all of the existing methods use the same spatial resolution, i.e., the same field of view, to measure two targets. Examples of these are listed as follows: (1) Two-channel systems with the same spatial resolution which measure the first derivative in the x- and y-directions. In these systems, the two channels correspond to two shearographic systems, one in the x-shearing direction to measure the first derivative of deformation in the x-direction and one in the y-shearing direction to measure the first derivative of deformation in the y-direction. Three methods have been reported to separate the information from these two channels in the final results. The first one is to use a two-camera system to record the information of the two channels separately [12]. The second method is to observe different channels on one color camera using RGB channels in combination with different laser wavelengths [13]. The last method is to use one black/white camera based on the polarization technology to avoid cross-interference [14,15]. These types of two-channel digital shearographic systems can be useful for NDT because some defects are sensitive to different directions of the first derivative of deformation. (2) The second example is a two-channel system with the same spatial resolution that simultaneously measures the deformation and its first derivative. For these systems, one channel is related to a holographic/electronic speckle pattern interferometry (ESPI) system and the other is related to a shearographic system [16–18]. Such kinds of systems are used if both the deformation and its derivative are needed at the same time. (3) Our last example is two-channel systems with the same spatial resolution that simultaneously measure both out-of-plane and in-plane strains. In these systems, one channel is used for an out-of-plane shearographic system and the other for an in-plane shearographic system [19,20]. They are usually utilized for 3D strain measurements.

Another application of two-channel systems is to test only one measurement target, but with different spatial resolutions. A Sagnac interferometer-based digital shearography system has been reported by Boyang Zhang et al. [21]. They used a Sagnac interferometer-based optical layout to enable a dual spatial resolution shearography system to measure the first derivative of deformation. It was the first recorded report of a system that allows two shearograms, one for a large field of view and one for a small field of view, to be obtained simultaneously. The development of this technology advanced digital shearography for NDT. However, a deficiency of the developed technology is the phenomenon of spectrum aliasing because the two shearograms have the same shearing direction, e.g., in the x-shearing direction, and all the spectra lie on the x-axis. In shearography, the orientation and separation of the spectrum are determined by the shearing direction and shearing amounts, respectively. Avoiding the spectrum aliasing of the two shearograms requires careful selection and adjustment of the shearing amount of the two channels, which complicates the measurement. Xiaowan Zheng reported an improved method to place one spectrum on the x-axis and the other on the y-axis to avoid the overlap [22]. However, this system is a two-target measurement, i.e., one channel measures the x-direction derivative and the other channel measures the y-direction derivative.

As described above, almost all of the simultaneous two-channel systems are based on digital shearography and for two target measurements because shearography can easily create two measurement targets, e.g., the first derivatives in the x- and y- directions, respectively. While the measurement of the first derivative of deformation has benefits for NDT, measuring deformation is as important as measuring the first derivative in the area of experimental mechanics, sometimes even more important because deformation is the basic behavior of an object after loading. Measuring a large-sized object with a high spatial resolution is always desired in the areas of experimental mechanics and non-destructive testing. In the past few years, a technology to enhance the spatial resolution by continuous-wave terahertz high-resolution imaging via synthetic technology has been achieved [23–25]. This technology can reach an extremely high spatial resolution with dozens of micrometers and has been proven to improve the reconstructed image quality and resolving power. Although the proposed technique can be employed in numerous domains, its application to experimental mechanics and non-destructive testing for processing directly recorded images in holographic and speckle interferometry with a close to real-time measurement speed for relatively large objects (one hundred to several hundred millimeters in diameter) is limited due to the complicated synthetic and reconstructing technologies. Another approach to reach a high spatial resolution is to use a dual-spatial-resolution shearographic system based on the Sagnac interferometer to measure the derivative of deformation as already described above. However, the Sagnac interferometer is relatively complicated in optics; furthermore, the system reported is not very practical due to the phenomenon of spectrum aliasing.

In this paper, we will present a novel dual-spatial-resolution holographic system to measure deformation, which has a relatively simple optical setup and can easily separate the spectra from two channels. By changing the combined focus length, the two holographic setups can observe different fields of view, i.e., one has a large and the other has a small field of view. To realize a simultaneous measurement, the polarization technique is used to avoid cross-interference between the two optical layouts [26]. Finally, based on the spatial carrier frequency technique [27], the reference beam is adjusted to introduce a different carrier frequency to obtain the spatial carrier fringes with different orientations in one speckle pattern image captured from the two holographic setups. The different oriented spatial carrier fringes enable the spectra of the two interferograms to be easily separated after a FT (Fourier transform), thus overcoming the main deficiency of spectrum aliasing reported in the dual-spatial-resolution shearographic system. The phase distributions of the two interferograms can be extracted and separated by windowing the spectrum to perform an IFT (inverse Fourier transform). The phase distributions can then be used to analyze and calculate the deformations. Different applications will be presented, and the practicability of this method is verified by the obtained experimental results.

2. Principle and Method

Our objective to develop a dual-resolution system is to obtain full and local measurement results simultaneously. Figure 1 shows the advantages of a dual-spatial-resolution system for NDT applications. From Figure 1a, a whole field can be observed under the large field of view, but minor defects that can be detected under the small field of view (Figure 1b) cannot be found under the large field of view.

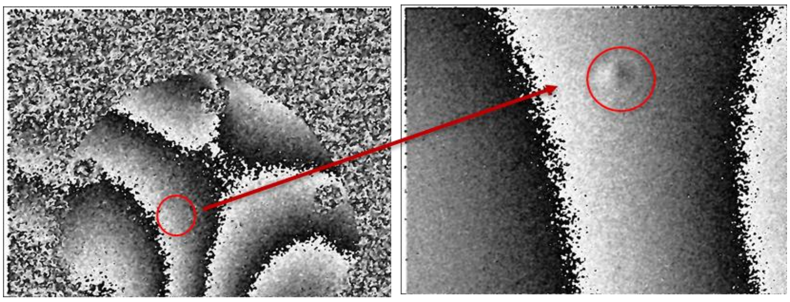
(a) (b)

Figure 1. Measuring results under different fields of view. (**a**) Fringe pattern under large field of view. (**b**) Fringe pattern under small field of view.

Figure 2 shows an optical setup to achieve simultaneous dual-resolution sensitivity measurements. The setup consists of a holography system using the multiple-carrier-frequency spatial-phase-shift method combined with the polarization technique. The laser beam is split by beam splitter 1 (BS1) into two beams, an object beam and a reference beam. The object beam goes to the object's surface, then is expanded through a beam expander (BE). Here, L1 to L4 are lenses with different focus lengths. Lens 1 (L1) is the image lens. Lens 2 (L2) and Lens 3 (L3) have the same focal length and are used to enlarge the field of view [28–30]. Lens 4 (L4) can enlarge the image to obtain a small field of view. The aperture (AP), placed just before the image lens (L1), is used to control the speckle size and spectrum pattern size on the Fourier domain. Beam splitter 2 (BS2) and beam splitter 3 (BS3) are beam splitters with a 50:50 ratio. Polarized beam splitter 1 (PBS 1) is a polarized beam splitter which can generate two non-coherent polarized object beams. Polarized beam splitter 2 (PBS2) is used to obtain two non-coherent polarized reference beams. The quarter-wave plate (QWP) can convert linearly polarized light to circular polarized light. A single-mode optical coupler (SOC) 50:50 splitter is used to split the reference beam into two beams that are both circular lights.

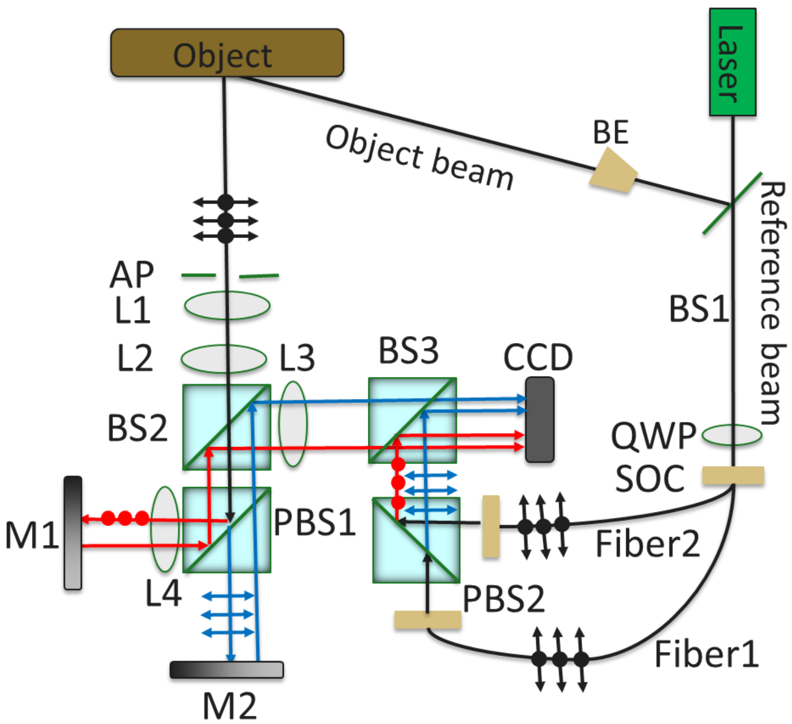

Figure 2. Sketch of simultaneous dual-resolution measurement system.

A frequency-doubled Nd: YAG laser (532 nm green) is used in the system. The laser is separated into an object beam and reference beam by using beam splitter 1 (BS1). The object beam is expanded by a beam expander (BE), and illuminates the object. The diffused object's light is reflected from the object, which is a circular light represented by a black line, then goes through the aperture (AP), image lens (L1), and lens L2 before arriving at the PBS. Here, the object beam is divided into two non-coherent polarized beams represented in red and blue, respectively. The red beam, or S-polarized light, is reflected by the PBS and goes through L4. It is then reflected by Mirror 1 (M1) before going into PBS1 again. After being reflected by PBS1 and BS2, the light goes through L3 and BS3 and is received by the CCD camera. The blue beam, or P-polarized light, goes through PBS1, then is reflected by mirror 2 (M2) before going into PBS1 again. The light is reflected by BS2, then goes through L3 and BS3 before arriving at the CCD camera.

The reference beam goes through a quarter-wave plate (QWP) and is converted into circular lights. It then goes into a single-mode optical coupler splitter fiber (OCS), in which the reference light is split into two identical circular lights represented by black lines. These two beams propagate through two optical fibers, then arrive at polarized beam splitter 2 (PBS2). Here, these two circular lights are converted to two non-coherent polarized lights which are represented by red and blue lines. These two polarized reference beams are independent. Different carrier frequencies can be introduced by adjusting the reference beams separately. The red line, or S-polarized light, is reflected by PBS2 and goes into BS3, where it is reflected before being received by the CCD camera. The blue line, representing P-polarized light, goes through PBS2 and is reflected by BS3 before arriving at the CCD camera. Here, the blue, P-polarized object and reference beams interfere with one another, and the red, S-polarized object and reference beams interfere with one another.

Through the design described above, the first two main goals of this research paper are been realized: (1) Two in-coherent holographic setups without cross-interference have been built in a multiplexed measurement setup, with each setup being independent and consisting of an object beam and reference beam which are split into two pairs of polarized beams; (2) the two optical channels have different fields of view, large and small. The red-S-polarized light goes through one more lens (L4) than the blue-P-polarized light, and the fields of view between the two channels can be adjusted by the focus length of L4. Next, we will discuss how to separate the measuring results from a single image recorded by one camera.

The carrier frequency used to obtain the frequency shift on the Fourier domain can be introduced by adjusting the two reference beams to change the incident angle from the normal of the CCD plane [30]. The hologram of the large field of view is generated by interference between the blue polarized object beam and reference beam, which both represent P-polarized light. The hologram of the small field view is also obtained through interference between the red polarized object beam and the red reference beam, both S-polarized light. The holograms of the large and small fields of view are simultaneously recorded by the CCD camera in the form of an intensity difference.

These two reference beams and two object beams' wave fronts can be represented by Equations (1)–(4):

$$u_{r1} = |u_{r1}(x,y)|exp\left\{i\left[2\pi\left(f_{1_x}x + f_{1_y}y\right)\right]\right\} \tag{1}$$

$$u_{r2} = |u_{r2}(x,y)|exp\left\{i\left[2\pi\left(f_{2_x}x + f_{2_y}y\right)\right]\right\} \tag{2}$$

$$u_{o1} = |u_{o1}(x,y)|exp[i\phi_1(x,y)] \tag{3}$$

$$u_{o2} = |u_{o2}(x,y)|exp[i\phi_2(x,y)] \tag{4}$$

where $u_{\mathrm{r}1}$ is the wave front of the red polarized reference beam, $u_{\mathrm{r}2}$ is the wave front of the blue polarized reference beam, u_{o1} is the wave front of the red polarized object beam, and u_{o2} is the wave front of the blue polarized object beam. The values f_{1x}, f_{1y}, f_{2_x}, and f_{2_y} represent the components of the spatial frequency. f_{1_x} and f_{1_y} are introduced by angle α_2

between the red polarized reference beam and the normal of the CCD plane, while f_{2_x} and f_{2_y} are introduced by angle β_2 between the blue polarized reference beam and the normal of the CCD plane. These components can be expressed as Equations (5)–(8), where λ is the laser wavelength:

$$f_{1_x} = \frac{sin\alpha_{2x}}{\lambda} \tag{5}$$

$$f_{1_y} = \frac{sin\alpha_{2y}}{\lambda} \tag{6}$$

$$f_{2_x} = \frac{sin\beta_{2x}}{\lambda} \tag{7}$$

$$f_{2_y} = \frac{sin\beta_{2y}}{\lambda} \tag{8}$$

The intensity image of both large and small fields of view can be recorded on the CCD camera simultaneously. u_{r1} and u_{r2}, as well as u_{o1} and u_{o2}, are non-coherent polarized lights. u_{r1} and u_{o1} are both S-polarized lights, represented by red lines, that interfere together to obtain the hologram for the small field of view, while u_{r2} and u_{o2} are P-polarized lights, represented by blue lines, that result in the hologram of the large field of view when they interfere with each other. The intensity recorded can be expressed as follows:

$$I_S = (u_{r1} + u_{o1})(u_{r1}{}^* + u_{o1}{}^*) = u_{r1}u_{r1}{}^* + u_{o1}u_{o1}{}^* + u_{r1}u_{o1}{}^* + u_{o1}u_{r1}{}^* \tag{9}$$

$$I_L = (u_{r2} + u_{o2})(u_{r2}{}^* + u_{o2}{}^*) = u_{r2}u_{r2}{}^* + u_{o2}u_{o2}{}^* + u_{r2}u_{o2}{}^* + u_{o2}u_{r2}{}^* \tag{10}$$

$$I = u_{r1}u_{r1}{}^* + u_{r2}u_{r2}{}^* + u_{o1}u_{o1}{}^* + u_{o2}u_{o2}{}^* + u_{r1}u_{o1}{}^* + u_{o1}u_{r1}{}^* + u_{r2}u_{o2}{}^* + u_{o2}u_{r2}{}^* \tag{11}$$

The * denotes the complex conjugate of u_{r1}, u_{r2}, u_{o1}, and u_{o2}. I_S and I_L are the intensity of the small field of view and the large field of view, respectively, while I is the total intensity recorded by the CCD camera. The intensity image is converted to the Fourier domain to obtain the phase information by applying a Fourier transform to I. Equation (11) is transformed into the following form:

$$\mathrm{FT}(I) = U_{r1} \otimes U_{r1}{}^* + U_{r2} \otimes U_{r2}{}^* + U_{o1} \otimes U_{o1}{}^* + U_{o2} \otimes U_{o2}{}^* + U_{r1} \otimes U_{o1}{}^* + U_{o1} \otimes U_{r1}{}^* + U_{r2} \otimes U_{o2}{}^* + U_{o2} \otimes U_{r2}{}^* \tag{12}$$

Here $\otimes$ is the convolution operation, $U_{r1} = \mathrm{FT}(u_{r1})$, $U_{r2} = \mathrm{FT}(u_{r2})$, $U_{o1} = \mathrm{FT}(u_{o1})$, and $U_{o2} = \mathrm{FT}(u_{o2})$.

Figure 3 shows a sketch of the Fourier spectrum of the intensity images. Five spectra are distributed on the Fourier domain, corresponding to the eight terms in Equation (12). Sections A contains $U_{r1} \otimes U_{r1}{}^* + U_{r2} \otimes U_{r2}{}^* + U_{o1} \otimes U_{o1}{}^* + U_{o2} \otimes U_{o2}{}^*$, which are low-frequency components that represent the background in the spatial domain. Sections B and C represent the $U_{r2} \otimes U_{o2}{}^*$ and $U_{o2} \otimes U_{r2}{}^*$ parts, respectively, which contain information of the hologram for the large field of view. Sections D and E represent the $U_{r1} \otimes U_{o1}{}^*$ and $U_{o1} \otimes U_{r1}{}^*$ parts, respectively. These two parts contain information of the hologram for the small field of view.

$u_{o1}u_{r1}{}^*$ can be obtained by employing an inverse Fourier transform to window the spectrum of $U_{o1} \otimes U_{r1}{}^*$. Similarly, $u_{o2}u_{r2}{}^*$ can be obtained using the same method. These results are shown in the following equations:

$$\phi_1(x, y) - 2\pi\left(f_{1_x}x + f_{1_y}y\right) = tan^{-1}\frac{\mathrm{Im}\left[u_{o1}u_{r1}^*\right]}{\mathrm{Re}\left[u_{o1}u_{r1}^*\right]} \tag{13}$$

$$\phi_2(x, y) - 2\pi\left(f_{2_x}x + f_{2_y}y\right) = tan^{-1}\frac{\mathrm{Im}\left[u_{o2}u_{r2}^*\right]}{\mathrm{Re}\left[u_{o2}u_{r2}^*\right]} \tag{14}$$

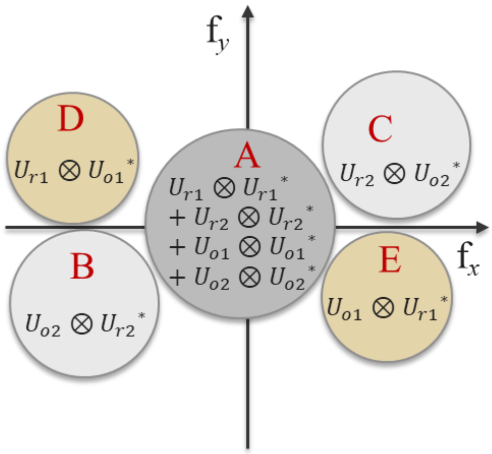

Figure 3. Sketch of the Fourier spectrum.

Using the same method, after the object deforms, the distribution of an additional two phases can be obtained, as described in the following equations:

$$\phi_1{}'(x,y) - 2\pi\left(f_{1_x}x + f_{1_y}y\right) = tan^{-1}\frac{\mathrm{Im}\left[u_{o1}u_{r1}^*\right]}{\mathrm{Re}\left[u_{o1}u_{r1}^*\right]} \tag{15}$$

$$\phi_2{}'(x,y) - 2\pi\left(f_{2_x}x + f_{2_y}y\right) = tan^{-1}\frac{\mathrm{Im}\left[u_{o2}u_{r2}^*\right]}{\mathrm{Re}\left[u_{o2}u_{r2}^*\right]} \tag{16}$$

The relative phase difference in the large and small fields of view due to a deformation resulting from an applied load can then be calculated as follows:

$$\Delta\phi_S = \phi_1{}'(x,y) - \phi_1(x,y) \tag{17}$$

$$\Delta\phi_L = \phi_2{}'(x,y) - \phi_2(x,y) \tag{18}$$

Through the operation described above, our last goal, i.e., to separate the phase information from the two holographic setups recorded in a single image by a Fourier transform and inverse Fourier transform, is attained, and the deformations of the large and small fields of view resulting from the applied load can then be calculated by the determined phase distribution. It should be emphasized that the direction of the carrier frequency in the holographic system determines the orientation of the spectrum of the hologram after the Fourier transform. A special advantage of holography is that a direction change in the carrier frequency can easily be implemented by adjusting the incident angle of the reference beams; therefore, the spectrum aliasing reported in the shearographic system [20] can be solved easily in the dual-channel holographic system.

3. Experiments and Results

Figure 4 shows a simultaneous dual-spatial-resolution digital holography measurement system. This system utilizes a Verdi G5 laser as well as a 2453 × 2056-pixel grayscale CCD camera. The pixel sizes of the CCD camera in the horizontal direction and the vertical directions are both 3.45 µm. L1, L2, L3, and L4 are the lenses. The focal lengths of the imaging lens, L1, is 35 mm (f_1 = 35 mm). The focal lengths of L2 and L3, placed on the two sides of the beam splitter, are 100 mm ($f_2 = f_3$ = 100 mm), and the focal length of L4 is 150 mm (f_4 = 150 mm). The normal beam splitter and polarized beam splitter both have split ratios of 50:50. The single-mode optical coupler splitter is 50:50.

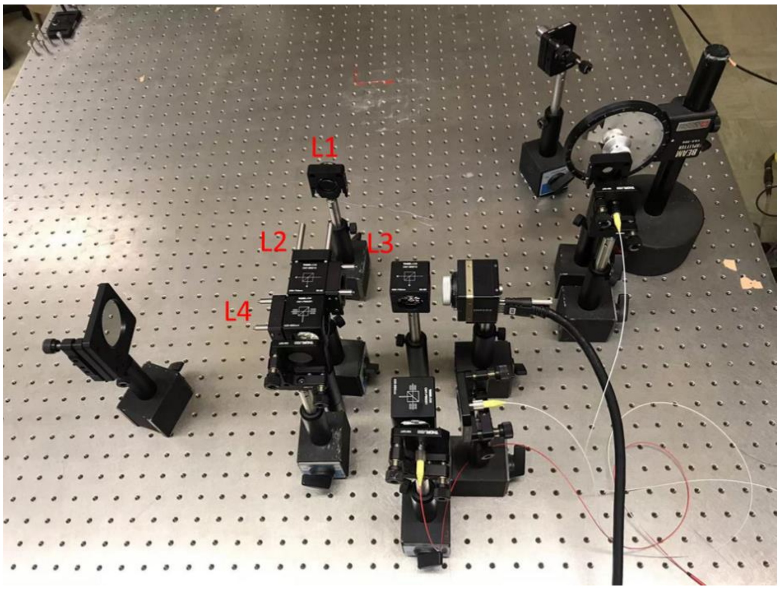

Figure 4. Experiment setup.

The measurement procedure is as follows: (1) to take an image before the loading, (2) to load the object, and (3) to take an image again after the loading, then, to conduct an evaluation of the measured result by Fourier and inverse Fourier transforms. The time for the measurements is determined by steps 1 to 3. Taking two images requires just dozens of milliseconds and the loading can be conducted within dozens of seconds, therefore, the whole measurement can be performed within one minute.

A 100 × 100 mm square aluminum plate was tested to verify the feasibility of the method. The plate was fixed along its four edges. A screw micrometer was used to apply a load to the center of the plate, and images before and after loading were captured for evaluation. A spectrum distribution was obtained, as shown in Figure 5a, by applying a FT. Then two holograms of two resolutions, as shown in Figure 5b,c, were obtained by using an IFT to obtain the phase information and subtracting the phase value before and after loading.

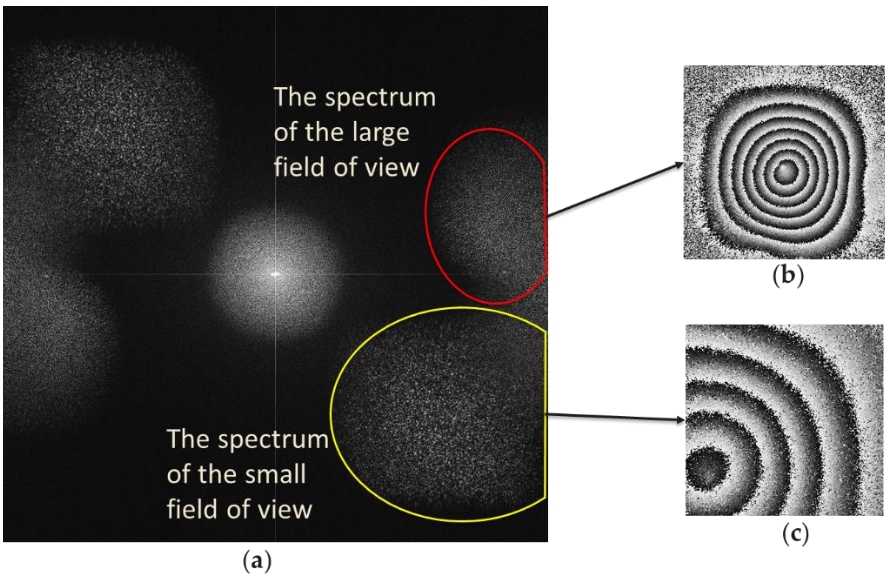

Figure 5. Schematic of spectrum of speckle pattern image: (**a**) is the spectrum, (**b**) is the hologram of large field of view, and (**c**) is the hologram of small field of view.

To verify the functionality of the digital holography system presented in this paper, an NDT application was performed on a round aluminum plate with a small-sized defect inside. The round plate had a thickness of 10 mm and was fixed on a 150 mm diameter sealed chamber. The sealed chamber was connected to a vacuum to load the round plate. The defect was a small circle with an 8 mm diameter and 0.6 mm of thickness to the surface. A 10 KPa pressure difference was applied to detect the defect, the result of which is shown in Figure 6. From the image, we can find that the whole area can be observed using the large field of view, but, as shown in Figure 6a, the small-sized defect may be ignored. However, the small-sized defects can be found under the small field of view, as shown as Figure 6b.

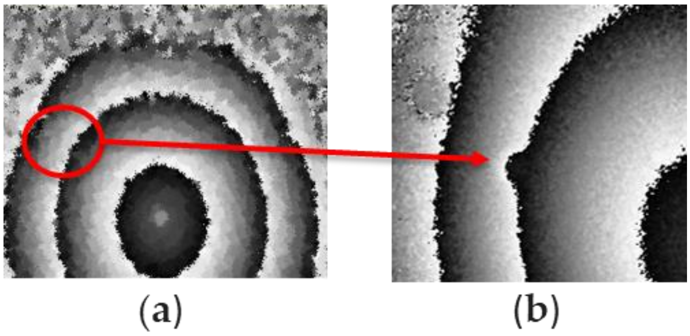

Figure 6. Hologram with defect using different field of view sizes. (**a**) Hologram of large field of view, (**b**) Hologram of small field of view.

Another deformation test was completed using this system and a defect-free square aluminum plate. The plate was fixed all around with screws, and the plate size was 100 × 100 mm. Figure 7 shows the phase map for the large field of view and small field of view, respectively. A load was applied at the center of the plate by a screw micrometer. Under the large field of view, the phase map, shown in Figure 7a, was very unclear because the large magnitude of the load caused the fringes to be too dense; as a result, it cannot be used to calculate the deformation. However, under the small field of view, the phase map, shown in Figure 7b, was clearer and could be used to calculate the deformation.

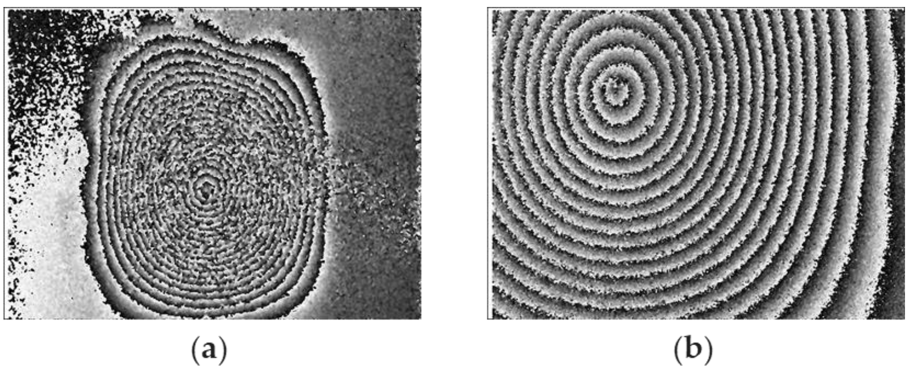

Figure 7. Phase map under large and small fields of view. (**a**) Phase map of large field of view, and (**b**) Phase map of small field of view.

4. Discussion

4.1. Adjustment of the System

Figure 8 shows the optical layouts of the two holographic setups. Figure 8a shows the setup for the large field of view and the Figure 8b shows the setup for the small field of view. The difference between them is L4, as L4 is introduced to enlarge the image to obtain the small field of view. The size of the small field of view can be changed by adjusting the position and changing the focus length of L4, and while the size of the large field of view can be adjusted by adjusting the position and changing the focus length of L1.

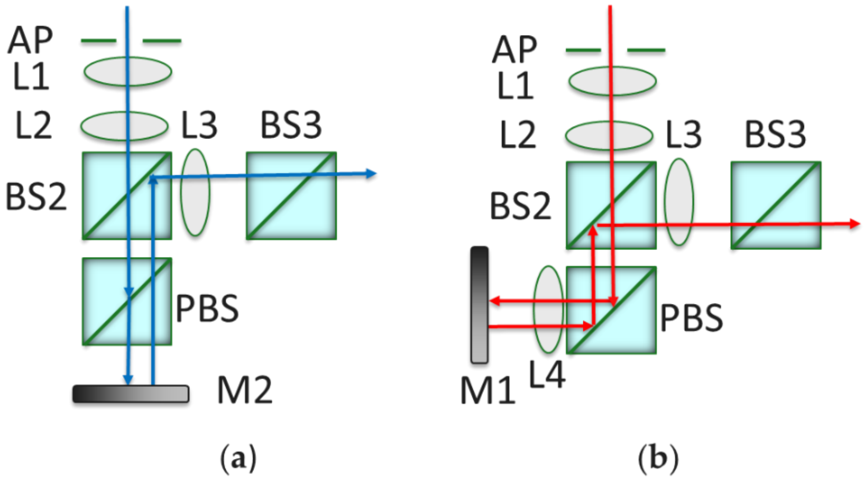

Figure 8. Sketch of two optical channels for two fields of view. (**a**) Optical channel for large field of view, and (**b**) Optical channel for small field of view.

The image with the large field of view must be adjusted first to make both of the different fields of view form clear images on the image plane. Adjusting the image with the large field of view is relatively easy. Adjusting the image with the small field of view on the same image plane is more challenging. It can be performed by adjusting the position of L4 in combination with that of mirror 1. Thus, it is important that mirror 1 should be able to be moved in the left and right directions.

4.2. Separate the Spectrums

After adjusting the two images with different fields of view into clear images on the image plane, it is also very important to adjust the reference beam of the two holographic setups to appropriate incident angles and planes. This is performed by introducing carrier fringes into the holograms. The two spectra transferred from the intensity images of the holograms should be separated to obtain good-quality phase maps. The orientation of the spectrum is determined by the direction of the carrier frequency. The advantage of the holographic system is the ease in changing the directions of carrier frequency; changing the direction is performed by adjusting the plane of the incident angle of the reference beam. The directions of the two carrier fringes should be checked before the Fourier transform is conducted. They should be orientated in different directions with a separation of at least 30 degrees. Figure 9 shows an ideal adjustment, in which the separation of the directions of the two carrier fringes is almost 90 degrees, resulting in two perfect mutually perpendicular spectrums. The phase distributions of the two holograms can then be easily separated by the inverse Fourier transform.

The size of the aperture of the camera is also important. A big aperture size leads to more light intensity going through the lens, allowing a relatively large object to be tested. This is desired in practical applications. However, a big aperture size results in a small speckle size. According to the sampling theorem, the speckle size should cover at least two pixels theoretically [31] and two to three times more practically, or at least four to six pixels [32]. Therefore, the aperture of the camera cannot be too big. Two adjustments can be performed to ensure a good measuring result with the small aperture: (1) enhancing the laser power to increase the light intensity to allow a relatively small aperture size to be used, and (2) using a CCD camera with a high resolution that has a relatively small pixel size to allow speckling, which results in covering more pixels.

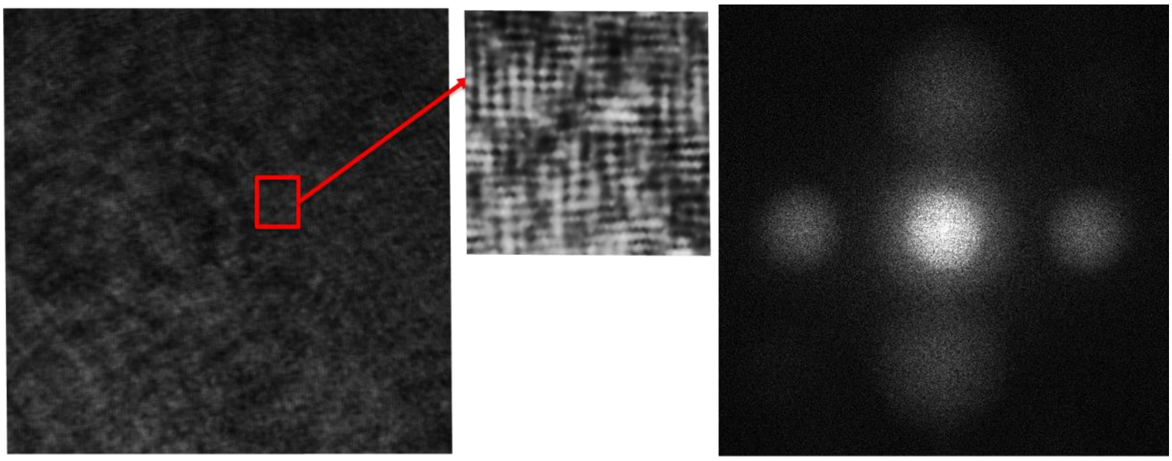

Figure 9. (**a**) Intensity image of an interferogram with carrier fringes, the area of the rectangle is magnified to show the carrier fringe. (**b**) Distribution of the spectrum.

5. Conclusions

A multiplexed holographic system for simultaneous dual-spatial-resolution measurements of deformation is presented in this paper. The main innovation of our research is we are the first to enable the digital holographic system to take simultaneous measurements with both the large and small fields of view and to observe whole-field deformations as well as local information, such as in the areas of strain concentration. The developed system is beneficial for deformation and strain measurements as well as for non-destructive testing, especially if the loading is not repeatable. The polarization technique is used to obtain two polarized holographic setups with two different-sized fields of view, large and small, by changing the combined focus length. The phase distributions of two holograms have been successfully extracted from one image containing two holograms recorded by a single camera through the spatial carrier fringes' phase shift method. The optical setup is relatively simple and the spectrums of two holograms can be separated easily by adjusting the orientation of the carrier fringes. This along with the good measurement results obtained from the setup increase its utility for practical applications. The special advantage of the system developed is its capability to perform simultaneous and dual-resolution measurements. This is particularly meaningful for some experiments which cannot be repeated; additionally, this can also lead to reduced labor and time costs associated with testing. The experiments conducted have demonstrated that the developed system is an effective tool to measure both whole and local information, especially in cases in which more detailed information is required for areas with a strain concentration and in cases in which smaller defects need to be found.

Author Contributions: Conceptualization, L.Y. and X.Z.; methodology, X.Z. and L.Y.; validation, X.Z., B.G. and S.F.; formal analysis, X.Z.; investigation, X.Z. and B.G.; resources, S.F. and B.S.; writing—original draft preparation, X.Z.; writing—review and editing, L.Y. and B.S.; supervision, L.Y.; project administration, X.Z. and L.Y. All authors have read and agreed to the published version of the manuscript.

Funding: This research received no external funding.

Informed Consent Statement: Not applicable.

Data Availability Statement: Data sharing not applicable.

Conflicts of Interest: The authors declare no conflict of interest.

References

1. Yang, L.; Xie, X. *Digital Shearography: New Developments and Applications*; SPIE Press: Washington, DC, USA, 2016.
2. Zhang, B.; Zheng, X.; Xu, W.; Yang, L. Overview of digital shearography for NDT. *Mater. Eval.* **2020**, *78*, 343–351. [CrossRef]
3. Wang, B.; Zhong, S.; Lee, T.L.; Fancey, K.S.; Mi, J. Non-destructive testing and evaluation of composite materials/structures: A state-of-the-art review. *Adv. Mech. Eng.* **2020**, *12*, 1687814020913761. [CrossRef]
4. Gupta, R.; Mitchell, D.; Blanche, J.; Harper, S.; Tang, W.; Pancholi, K.; Baines, L.; Bucknall, D.G.; Flynn, D. A review of sensing technologies for non-destructive evaluation of structural composite materials. *J. Compos. Sci.* **2021**, *5*, 319. [CrossRef]
5. Raj, B.; Jayakumar, T.; Thavasimuthu, M. *Practical Non-Destructive Testing*; Woodhead Publishing: Cambridge, UK, 2002.
6. Gryzagoridis, J.; Findeis, D. Impact damage detection on composites using optical NDT techniques. *Insight-Non-Destr. Test. Cond. Monit.* **2010**, *52*, 248–251. [CrossRef]
7. Hariharan, P. *Basics of Holography*; Cambridge University Press: Cambridge, UK, 2002.
8. Ettemeyer, A. Combination of 3-D deformation and shape measurement by electronic speckle pattern interferometry for quantitative strain-stress analysis. *Opt. Eng.* **2000**, *39*, 212–215. [CrossRef]
9. Collier, R. *Optical Holography*; Elsevier: Amsterdam, The Netherlands, 2013.
10. Ulf, S.; Falldorf, C.; Watson, J.; Jüptner, W. *Digital Holography*; Springer: Berlin/Heidelberg, Germany, 2015.
11. Liu, B.; Wang, S.; Zhan, M.; Wang, H.; Zhang, G.; Jian, Q. Optical nondestructive evaluation for minor debonding defects and interfacial adhesive strength of solid propellant. *Measurement* **2022**, *194*, 111066. [CrossRef]
12. Steinchen, W.; Yang, L. *Digital Shearography: Theory and Application of Digital Speckle Pattern Shearing Interferometry*; SPIE Press: Bellingham, WA, USA, 2003; Volume 93.
13. Richoz, G.L.; Schajer, G.S. Simultaneous two-axis shearographic interferometer using multiple wavelengths and a color camera. *Opt. Lasers Eng.* **2016**, *77*, 143–153. [CrossRef]
14. Siebert, T.; Schmitz, B. New shearing setup for simultaneous measurement of two shear directions. In *Practical Holography XIII*; SPIE: Washington, DC, USA, 1999; Volume 3637, pp. 225–230.
15. Xie, X.; Lee, C.P.; Li, J.; Zhang, B.; Yang, L. Polarized digital shearography for simultaneous dual shearing directions measurements. *Rev. Sci. Instrum.* **2016**, *87*, 083110. [CrossRef]
16. Bhaduri, B.; Mohan, N.K.; Kothiyal, M.P. Simultaneous measurement of out-of-plane displacement and slope using a multiaperture DSPI system and fast Fourier transform. *Appl. Opt.* **2007**, *46*, 5680–5686. [CrossRef]
17. Qihan, Z.; Chen, W.; Sun, F.; Yan, P.; Ye, B.; Wang, Y. Simultaneous 3D measurement of deformation and its first derivative with speckle pattern interferometry and shearography. *Appl. Opt.* **2019**, *58*, 8665–8672.
18. Hooshmand-Ziafi, H.; Hassani, K.; Dashtdar, M. Dual-sensitive spatial phase-shifting shearography based on a common-path configuration. *Opt. Eng.* **2019**, *58*, 114104. [CrossRef]
19. Francis, D.; Tatam, R.P.; Groves, R.M. Shearography technology and applications: A review. *Meas. Sci. Technol.* **2010**, *21*, 102001. [CrossRef]
20. Dong, J.; Wang, S.; Lu, M.; Jakobi, M.; Liu, Z.; Dong, X.; Pöller, F.; Bilgeri, L.M.; Bloise, F.S.; Yetisen, A.K.; et al. Real-time dual-sensitive shearography for simultaneous in-plane and out-of-plane strain measurements. *Opt. Express* **2019**, *27*, 3276–3283. [CrossRef] [PubMed]
21. Zhang, B.; Zheng, X.; Guo, B.; Fang, S.; Sia, B.; Yang, L. Sagnac interferometer based digital shearography for simultaneous dual sensitivity measurement. *Opt. Lasers Eng.* **2022**, *152*, 106984. [CrossRef]
22. Zheng, X.; Guo, B.; Fang, S.; Sia, B.; Yang, L. *Development of Digital Shearography for Dual Sensitivity Simultaneous Measurement Using Carrier Frequency Spatial Phase Shift Technology*; No. 2023-01-0068; SAE Technical Paper: Warrendale, PA, USA, 2023. Available online: https://www.sae.org/publications/technical-papers/content/2023-01-0068/ (accessed on 9 February 2023).
23. Huang, H.; Qiu, P.; Panezai, S.; Hao, S.; Zhang, D.; Yang, Y.; Ma, Y.; Gao, H.; Gao, L.; Zhang, Z.; et al. Continuous-wave terahertz high-resolution imaging via synthetic hologram extrapolation method using pyroelectric detector. *Opt. Laser Technol.* **2019**, *120*, 105683. [CrossRef]
24. Huang, H.; Rong, L.; Wang, D.; Li, W.; Deng, Q.; Li, B.; Wang, Y.; Zhan, Z.; Wang, X.; Wu, W. Synthetic aperture in terahertz in-line digital holography for resolution enhancement. *Appl. Opt.* **2016**, *55*, A43–A48. [CrossRef]
25. Li, Z.; Yan, Q.; Qin, Y.; Kong, W.; Li, G.; Zou, M.; Wang, D.; You, Z.; Zhou, X. Sparsity-based continuous wave terahertz lens-free on-chip holography with sub-wavelength resolution. *Opt. Express* **2019**, *27*, 702–713. [CrossRef]
26. Wang, Y.; Gao, X.; Xie, X.; Wu, S.; Liu, Y.; Yang, L. Simultaneous dual directional strain measurement using spatial phase-shift digital shearography. *Opt. Lasers Eng.* **2016**, *87*, 197–203. [CrossRef]
27. Kujawinska, M.; Wojciak, J. Spatial-carrier phase-shifting technique of fringe pattern analysis. In *Industrial Applications of Holographic and Speckle Measuring Techniques*; SPIE: Washington, DC, USA, 1991; Volume 1508, pp. 61–67.
28. Goldberg, K.A.; Bokor, J. Fourier-transform method of phase-shift determination. *Appl. Opt.* **2001**, *40*, 2886–2894. [CrossRef]
29. Boudebs, G.; Besse, V.; Cassagne, C.; Leblond, H.; de Araújo, C.B. Nonlinear characterization of materials using the D4σ method inside a Z-scan 4f-system. *Opt. Lett.* **2013**, *38*, 2206–2208. [CrossRef]
30. Schnars, U.; Kreis, T.M.; Jüptner, W.P. Digital recording and numerical reconstruction of holograms: Reduction of the spatial frequency spectrum. *Opt. Eng.* **1996**, *35*, 977–982. [CrossRef]

31. Pedrini, G.; Zou, Y.L.; Tiziani, H.J. Quantitative evaluation of digital shearing interferogram using the spatial carrier method. *Pure Appl. Opt. J. Eur. Opt. Soc. Part A* **1996**, *5*, 313. [CrossRef]
32. Xie, X.; Xu, N.; Sun, J.; Wang, Y.; Yang, L. Simultaneous measurement of deformation and the first derivative with spatial phase-shift digital shearography. *Opt. Commun.* **2013**, *286*, 277–281. [CrossRef]